IEEE Access
Multidisciplinary ⋮ Rapid Review ⋮ Open Access Journal

Received 27 August 2023, accepted 12 September 2023, date of publication 18 September 2023,
date of current version 29 September 2023.

Digital Object Identifier 10.1109/ACCESS.2023.3316716

RESEARCH ARTICLE

BLER and Throughput Analysis of Power Beacon-Based Energy Harvesting UAV-Assisted NOMA Relay Systems for Short-Packet Communications

TRAN MANH HOANG[1], LE THE DUNG[2], (Member, IEEE), BA CAO NGUYEN[3], NGUYEN VAN VINH[4], AND TAEJOON KIM[5,6], (Member, IEEE)

[1]Faculty of Telecommunications Services, Telecommunications University, Nha Trang 650000, Vietnam
[2]Faculty of Computing Fundamentals, FPT University, Ho Chi Minh City 700000, Vietnam
[3]Faculty of Basic Techniques, Telecommunications University, Nha Trang 650000, Vietnam
[4]Department of Artificial Intelligence, FPT University, Hanoi 100000, Vietnam
[5]Research Institute for Computer and Information Communication, Chungbuk National University, Cheongju 28644, South Korea
[6]School of Information and Communication Engineering, Chungbuk National University, Cheongju 28644, South Korea

Corresponding author: Taejoon Kim (ktjcc@chungbuk.ac.kr)

This work was supported by the Basic Science Research Program through the National Research Foundation of Korea (NRF) funded by the Ministry of Education under Grant RS-2023-00244014.

ABSTRACT In this paper, we analyze an unmanned aerial vehicle (UAV) that harvests energy from a power beacon to support the transmissions of finite blocklength packets from a source to two destinations using non-orthogonal multiple access (NOMA) scheme. The impacts of line-of-sight (LoS) and non-LoS communications on the block error rate (BLER) and throughput of the system are presented via the Rician factor. For the evaluation of system performance, we derive the closed-form and approximate expressions of the BLERs of each hop and the end-to-end communication path between source and destination. Based on these derived BLER expressions, we calculate the throughput of the considered UAV-NOMA-short packet communication (SPC) system. Analytical results are verified by Monte-Carlo simulations. Numerical results show that the best system performance can be achieved by selecting a reasonable time switching duration for energy harvesting, blocklength, and the number of training bits. The minimal BLERs can be obtained by controlling the trajectory of the UAV, i.e., its altitude and location on the horizontal plane. The BLER performance of the UAV-NOMA-SPC system is compared with that of the UAV-orthogonal multiple access (OMA)-SPC system, showing that the UAV-NOMA-SPC gives a lower average BLERs than the UAV-OMA-SPC system.

INDEX TERMS Unmanned aerial vehicle (UAV), non-orthogonal multiple access (NOMA), energy harvesting, successive interference cancellation (SIC), block error rate (BLER), throughput.

I. INTRODUCTION

Nowadays and soon, electrical devices are growing fast, as reported by Ericsson [1]. This report states that there will be around 36,048 connected devices in wireless communication by the year 2025, which will form the Internet-of-Thing (IoT) systems. Additionally, more interconnected devices operate intelligently, and the electric industry will become a hot trend and continue beyond 2030. Thus, wireless communication systems require much more resources and higher criteria such as latency lower than 0.1 ms, reliability higher than 99.99999%, and sensing accuracy at the millimeter-level. Besides, energy efficiency is a major problem in the fifth-generation (5G) and sixth-generation (6G) networks. To deal with these requirements, several solutions are suggested: 1) using the non-orthogonal multiple

The associate editor coordinating the review of this manuscript and approving it for publication was Guillermo Valencia-Palomo.

access (NOMA) to improve the spectrum efficiency in 5G and 6G systems [2], [3], 2) utilizing short packets to achieve ultra-reliable low latency communications (URLLC), which is helpful in the IoT systems, 3) employing unmanned aerial vehicles (UAVs) to provide dynamic mobility for the communication devices in disaster and emergency response, 4) applying energy harvesting to overcome the limited battery capacity of electric devices and UAV [4]. On the other hand, in the command-control and monitor systems for toxic areas, the usage of UAVs to communicate becomes the trend because it does not require fixed infrastructure [5], [6], [7], [8].

A. RELATED WORK

Recent investigations into UAV-assisted short-packet communications combined with energy harvesting have attracted much attention from researchers. In particular, Ranjha et al. [4] formulated a non-convex joint resource allocation, trajectory design, and energy harvesting problem to minimize the total decoding error rate in URLLC-enable laser-powered UAV relay systems. Raut et al. [9] investigated a nonlinear energy harvesting (EH)-based UAV-assisted FD relay network with infinite and finite blocklength codes, where source UAV harvested energy transmitted from a laser transmitter. The closed-form expression of block error rate (BLER) was derived under the impacts of imperfect channel state information (CSI). Agrawal et al. [10] analyzed the average outage probability, BLER, and goodput of reconfigurable intelligent surface (RIS)-assisted UAV-based multiuser communication system with finite blocklength codes and nonlinear EH of the ground user. Moreover, the investigation harvested energy for the UAV-assisted infinite blocklength communications have been studied in many works such as [11], [12], [13], [14], and [15]. These works stated that the harvested energy was enough for signal transmission.

On the other hand, UAV-assisted short-packet communication (SPC) systems without energy harvesting have also been considered in the literature. Particularly, Hu et al. [16] studied the influence of SPC on the performance of UAV-enable cognitive networks. The authors formulated the optimization problem for maximizing the energy efficiency under the constraints of packet error rate, spectrum sensing duration and threshold, and the transmit power of the UAV. Basnayaka et al. [17] studied the age of information of an URLLC-enable UAV wireless network by deriving the closed-form expression of this performance metric. Yuan et al. [18] derived the closed-form expression of BLER and applied both bisection search and one-dimensional search algorithm to maximize the energy efficiency of the UAV in a UAV-assisted URLLC between a base station and a user. The usage of short packets for remote control of the UAV was considered in [19], [20], and [22]. The authors derived closed-form expressions of the average packet error probability (APEP) and throughput of these systems. Ranjha et al. [21] performed passive beamforming of RIS antenna elements and nonlinear nonconvex optimization to minimize the overall decoding error rate and find the optimal UAV's position and blocklength. From Table 1,[1] we see that most of the above UAV-assisted SPC systems utilized orthogonal multiple access (OMA) schemes and did not use the energy harvesting technique. Only several works applied simultaneous wireless information and power transfer (SWIPT) to the UAV. However, SWIPT may not be an efficient EH technique for UAV-assisted communication systems.

Presently, incorporating the NOMA technique into SPC helps to improve the spectral efficiency of finite blocklength transmissions. Specifically, Yao et al. [23] proposed a join decoding for downlink NOMA systems with finite blocklength transmissions. Le et al. [24] studied an uplink NOMA wireless system with SPC under channel estimation errors and residual transceiver hardware impairments. The authors provided the average BLER in the finite blocklength regime, then formulated a maximum throughput optimization problem subject to the packet length. Comparisons between NOMA-SPC and OMA-SPC were also presented. Tran et al. [25] investigated a multi-user downlink MIMO-NOMA system with SPC. For evaluating the system performance, the authors derived the asymptotic and approximate closed-form expressions of the average BLER. Vu et al. [26] studied the performance of IRS-aided short-packet NOMA systems under perfect and imperfect SIC by deriving the closed-form approximated expressions of BLER with random and optimal phase shifts. Yin et al. [27] proposed a packet re-management framework for a cooperative NOMA scheme for SPC and gave a linear searching method to solve the problem of minimizing power consumption. It is worth noticing that the NOMA-SPC systems in [23], [24], [25], [26], and [27] did not consider the usage of UAVs despite of the advantages of using UAV such as high mobility and versatility. Additionally, energy charging for the UAV using a power beacon was also not considered in the above works. The main reason for these matters is the extreme difficulty in obtaining the closed-form mathematical expressions of the BLER and throughput of the EH-enable UAV-assisted NOMA-SPC system over Rician channels. Furthermore, since the UAV's propulsion energy is much higher than the UAV's communication energy in practice, the issue of compatibility between them occurs. On the other hand, utilizing the propulsion energy of a UAV for communication might introduce fluctuations in the signals. Moreover, using the energy of a UAV for information transmission would further drain the battery, reducing its operational time. To overcome these limitations, we mathematically study a UAV-assisted NOMA relay system where a UAV harvests energy from a power beacon to support short-packet transmissions over Rician channels. The main contributions of this paper are summarized as follows:

[1] PL is the log-distance path-loss, defined in detail in [1].

TABLE 1. Literature review on some related UAV-assited SPC systems.

Ref.	Channel Model	Access Scheme	Energy Harvesting	Role of UAV	Packet Type	Evaluating Metrics
[4]	PL	OMA	Yes	Relay	Finite	BLER
[9]	Rician	OMA	Yes	Source	Finite	BLER, Throughput
[10]	Rayleigh	OMA	Yes	Source	Finite	BLER, Throughput
[16]	PL	OMA	No	Source	Finite	Energy Efficiency
[17]	PL, Rician	OMA	No	Relay	Finite	Age of Information
[18]	PL, Rayleigh	OMA	No	Relay	Finite	BLER
[19]	PL	OMA	No	User	Finite	Rate
[20]	PL	OMA	No	User	Finite	BLER
[21]	PL, Rician	OMA	No	Relay	Finite	BLER
Our work	PL, Rician	NOMA	Yes	Relay	Finite	BLER, Throughput

- Unlike previous works which studied UAV-SPC systems without NOMA [4], [9], [10], [16], [17], [18], [19], [20], [21] or NOMA-SPC systems without UAV and EH [23], [24], [25], [26], [27], we fill these research gaps by investigating a UAV-assisted NOMA relay system, where an EH-enable UAV employs NOMA technique to forward finite blocklength packets from a source to two destinations (now called the UAV-NOMA-SPC system).
- We first derive the signal-to-interference-plus-noise ratio (SINR) expressions corresponding to the light-of-sight (LoS) and NLoS communications. Based on these SINR expressions, we provide the closed-form expressions of the performance in terms of the BLER and throughput of the considered UAV-assisted NOMA relay system with finite packet size. For practical UAV-assisted communications, we investigate the system performance over Rician fading channel and different urban environments.
- We extensively study the effects of energy harvesting duration, environments, the number of training bits, the 3D trajectory of the UAV, the Rician factor, and blocklength on the BLERs and throughput of the considered UAV-NOMA-SPC system. We show that the best system performance can be obtained by determining the appropriate energy harvesting duration, UAV coordinate, the number of training bits, and power allocation coefficient. The comparisons between the BLERs of the UAV-NOMA-SPC and UAV-OMA-SPC systems are also provided to show the advantage of the considered system.

The remainder of this paper is structured as follows. Section II describes the system model. Section III presents the mathematical analysis of the BLER and the throughput. The main results and relevant discussions are given in detail in Section IV. Finally, Section V concludes the paper.

Notation: $\mathbf{a}$ represents a vector while $\|a\|$ is the Euclidean norm of $\mathbf{a}$. $[\cdots]^T$ denotes the transpose of $[\cdots]$. $f_X(x)$ and $F_X(x)$ refer to the probability density function (PDF) and the cumulative distribution function (CDF) of a random variable X, respectively; $\|\cdot\|^2$ means the Frobenius norm; the expectation operator is $\mathbb{E}[\cdot]$.

II. SYSTEM MODEL

Fig. 1 illustrates the wireless-powered UAV-NOMA-SPC system considered in this paper. It consists of four nodes:

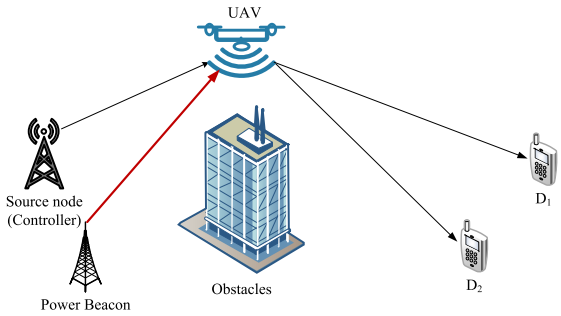

FIGURE 1. Illustration of a power beacon-based energy harvesting UAV-assisted NOMA relay system for short-packet communications.

a source node (S) as a controlling station, two destinations (D_1 and D_2), a UAV as an air relay (AR), and a power beacon (PB). It is assumed that the direct links between S and D_i are unavailable due to mountains or high-rise buildings. Thus, the communication between S and D_i is assisted by the UAV operating as a decode-and-forward (DF) relay. Moreover, the power for S and D_i come from a fixed power source, while the operating energy of the UAV is harvested from the PB [4]. Without loss of generality, we assume that S, PB, and D_i are located on a horizontal plane and the UAV hovers above them. Specifically, the locations of all nodes are $w_s = S(x_s, y_s, 0)$, $w_p = PB(x_p, y_p, 0)$, $w_1 = D_1(x_{w_1}, y_{w_1}, 0)$, $w_2 = D_2(x_{w_2}, y_{w_2}, 0)$, and UAV (x_u, y_u, H). In this paper, the flying time of the UAV from the initial point $q_I = (x_I, y_I, H)$ to the final point $q_F = (x_F, y_F, H)$ is T, and it is divided into N sub-timeslots, i.e., each incremental time of UAV is $\delta_t = \frac{T}{N}$. The location of the UAV at the nth time slot is expressed as UAV $q[n] = (x_u[n], y_u[n], H)$, $n \in \{1, \cdots, N\}$. The distance between PB and UAV at the nth time slot is $d_p = \sqrt{\|q[n] - w_p\|^2 + v\delta_t + H^2}$ while the distance between UAV and D_i is $d_i = \sqrt{\|q[n] - w_i\|^2 + v\delta_t + H^2}$. The sub-timeslot is formulated as $\delta_t = \frac{q[n+1]-q[n]}{v}$, where v is the velocity of UAV. When $n = 1$, the UAV stays right above S; when $n = N$, the UAV stays right above D_i. The incremental distance during each sub-timeslot δ_t must satisfy $\|q[n+1]-q[n]\|^2 \leq v\delta_t$ so that the location of UAV is almost unchanged during each sub-timeslot.

A. CHANNEL MODEL

The wireless channels are modeled by two kinds of fading, i.e., large-scale fading and small-scale fading. The large-scale

fading depends on the distance between transmitter and receiver and the path loss of the propagation environment. The amplitude of small-scale fading is fixed in one symbol duration but may be changed randomly over the next symbol. We denote the large-scale fading between S and the UAV as $\mathcal{L}_s[n] = \frac{\beta_0}{(\|q[n]-w_s\|^2+H^2)^\alpha}$, and from the UAV to D_i as $\mathcal{L}_d[n] = \frac{\beta_0}{(\|q[n]-w_i\|^2+H^2)^\alpha}$, and the distance between the PB and the UAV as $\mathcal{L}_p[n] = \frac{\beta_0}{(\|q[n]-w_p\|^2+H^2)^\alpha}$, where β_0 refers to the channel gain at the reference distance $d_0 = 1$ m [28] and $\alpha(\theta_\ell) = [\alpha(\frac{\pi}{2}) - \alpha(0)]\eta + \alpha(0)$, $\ell \in \{S, PB, D_i\}$ represents the path-loss coefficient from the UAV to ground users, $0 \le \eta \le 1$ is an additional attenuation factor to show the relationship between the LoS probability and the elevation angle of the UAV and ground terminals. The probabilities of LoS and NLoS links are, respectively, characterized as [29]

$$P_{LoS}(\theta_\ell) = c_1 - \frac{c_1 - c_2}{1 + \left(\frac{\theta_\ell - c_3}{c_4}\right)^{c_5}}, \tag{1}$$

$$P_{NLoS}(\theta_\ell) = 1 - P_{LoS}(\theta_\ell), \tag{2}$$

where $\theta_\ell = \frac{180^o}{\pi} arcsin(\frac{H}{d_\ell})$; c_k with $k \in \{1, \cdots, 5\}$ are constants, which depend on the types of urban environments. Their empirical values are presented in Table 2.

TABLE 2. Parameters for LoS probability calculation [29].

Environment	c_1	c_2	c_3	c_4	c_5
Suburban	101.6	0	0	3.25	1.241
Urban	120.0	0	0	24.30	1.229
Dense urban	187.3	0	0	82.10	1.478

Obviously, the altitude of the UAV influences the quality of signal propagation from ground users to the UAV, i.e., the LoS probability between ground users and the UAV depends on θ_ℓ. In particular, larger θ_ℓ (which also means higher altitude of the UAV) leads to higher LoS probability; however, the path losses of wireless links also increase.[2]

Due to the effects of LoS connections and multi-path scattering at ground users, the fluctuation of small-scale fading can be modeled by Rician distribution [31]. Let us denote h_s, h_p, h_{d_i} as the small-scale fading coefficients between S and UAV, PB and UAV, UAV and D_i, respectively. These are modeled as

$$h_\ell = \sqrt{\frac{K_\ell}{K_\ell + 1}}\sigma_\ell e^{j\phi} + \sqrt{\frac{1}{K_\ell + 1}}\mathcal{CN}(0, \sigma_\ell^2), \tag{3}$$

where the first term represents the specular path arriving with uniform phase ϕ and the second term refers to the aggregation of large numbers of reflected and scattered paths, which is independent of ϕ; $K_\ell = \frac{P_{LoS}(\theta_\ell)}{1-P_{LoS}(\theta_\ell)}$ is the Rician factor defined as the ratio of the power in the LoS component to the power in the multipath scatters [17], and $\mathcal{CN}(0, \sigma_\ell^2)$ is the random scattering component, which is a circularly symmetric complex Gaussian (CSCG) random variable with zero mean and unit variance. Note that K_ℓ only represents the possibility of having LoS communications in small-scale fading but does not include the path loss in large-scale fading. The probability distribution function (PDF) of h_ℓ is

$$f_{|h_\ell|^2}(x) = \frac{(K_\ell + 1)e^{-K_\ell}}{\lambda_\ell} \exp\left(-\frac{(K_\ell + 1)x}{\lambda_\ell}\right) \times I_0\left(2\sqrt{\frac{K_\ell(K_\ell + 1)x}{\lambda_\ell}}\right), x \ge 0, \tag{4}$$

where $I_0(\cdot)$ denotes the zero-order modified Bessel function of the first kind, $\lambda_\ell = \mathbb{E}|h_\ell|^2$ is the average channel gain of small-scale fading. Without loss of generality, the average channel gain of the system under the effects of both large-scale and small-scale fading can be presented as $\hat{\Omega}_\ell = \omega\lambda_\ell|\mathcal{L}_\ell[n]|$, where ω is an additional attenuation factor caused by the LoS or NLoS communications in large-scale fading. Notably, $\omega = 1$ for LoS communication and $0 < \omega < 1$ for NLoS communication [32]. This means that the average channel gains corresponding to LoS and NLoS communications between ground terminals and the UAV are given by [33]

$$\Omega_\ell = \begin{cases} (1-\rho)\hat{\Omega}_\ell & \text{LoS link,} \\ \omega(1-\rho)\hat{\Omega}_\ell & \text{NLoS link,} \end{cases} \tag{5}$$

where $0 < \rho \le 1$ reflects the impact of moving speed of the UAV [9], [34], [35]. In the case of uniform scattering, ρ can be calculated as $\rho = J_0\left(\frac{2\pi f_c v}{r_s c}\right)$, where f_c is the carrier frequency, c is the speed of light, r_s is the symbol rate, and $J_0(\cdot)$ is the for zeroth order Bessel function of the first kind. We can see that ρ affects the average channel gain, i.e., a larger ρ means the velocity v of the UAV is higher, leading to a smaller average channel gain. It is also assumed that the Doppler effect caused by the UAV mobility is perfectly compensated at the receivers [36], and the coherence time of a signal over a channel use is perfect.

Therefore, under the effects of both large-scale and small-scale fading, the channel between PB and UAV is $h_{pu} = \mathcal{L}_p[n]h_p$, between S and UAV is $h_{su} = \mathcal{L}_s[n]h_s$ and from UAV to D_i is $h_{ud_i} = \mathcal{L}_d[n]h_{d_i}$.

B. ENERGY HARVESTING AND COMMUNICATION MODEL

Regarding the energy harvesting process, the interval κ of each transmit symbol period is used to harvest energy from PB. During this duration, the UAV harvests energy transmitted from PB by using time switching (TS) protocol.[3] Thus, the harvested energy at the UAV in m channel use (cu) is [14], [37], and [38]

$$E_A = \kappa m P_b |h_{pu}|^2 \xi, \tag{6}$$

[2] As reported in [30], an A2G channel with perfect LoS probability can be achieved when the UAV altitude is larger than 40 m in the rural macrocell (RMa) scenario.

[3] In the TS model, higher SNR can be achieved at the cost of shorter blocklength for data transmission [9].

where P_b is the transmit power of PB and ξ denotes the energy conversion efficiency at the UAV. Since the UAV operates in half-duplex (HD) mode, the transmit power of the UAV is

$$P_r = \frac{2\kappa m\xi P_b|h_{pu}|^2}{1-\kappa} = \Delta|h_{pu}|^2, \text{ with } \Delta = \frac{2\kappa m\xi P_b}{1-\kappa}. \quad (7)$$

During the remaining symbol period, S transmits control signals to D_i in HD mode, i.e., S sends data blocks with the sizes of $m(1-\kappa)/2$ symbol to the UAV in the first phase; then the UAV forwards the control signals to D_1 and D_2 over remaining $m(1-\kappa)/2$ symbol. For the transmission of control signals, the number of codewords needs to be small to satisfy low latency. Thus, the length of the transmitted packet is finite. This setting is suitable for the communications and controls of coastal ships using finite blocklength codes.[4]

For the power-domain NOMA technique, in the first phase, S superposes x_1 and x_2 according to the power allocation coefficients a_1 and a_2, respectively, i.e, $x_S = \sqrt{a_1P_s}x_1 + \sqrt{a_2P_s}x_2$, $a_1 \le a_2$ and $a_1 + a_2 = 1$, where P_s is the transmit power of S. Consequently, the received signal at the UAV is

$$y_U = h_{su}(\sqrt{a_1P_s}x_1 + \sqrt{a_2P_s}x_2) + w_u, \quad (8)$$

where $w_u = \mathcal{CN}(0, \sigma_U^2)$ is the additive white Gaussian noise (AWGN) with zero mean and standard variance of σ_U^2 at the UAV. The signal x_2 is first decoded at the UAV and treated x_1 as noise, then the UAV decodes x_1 by applying SIC technique to subtract x_2. Thus, the signal-to-interference plus noise ratios (SINRs) of x_1 and x_2 in the case of perfect SIC are, respectively, expressed as

$$\gamma_{AR}^{x_2} = \frac{a_2P_s|h_{su}|^2}{a_1P_s|h_{su}|^2 + \sigma_{AR}^2}, \quad (9)$$

$$\gamma_{AR}^{x_1} = \frac{a_1P_s|h_{su}|^2}{\sigma_{AR}^2}. \quad (10)$$

In the second phase, the UAV re-superimposes $\hat{x}_1$ and $\hat{x}_2$ according to the power coefficients a_1 and a_2, respectively, i.e., $x_U = \sqrt{a_1P_r}\hat{x}_1 + \sqrt{a_2P_r}\hat{x}_2$. Thus, the received signals at both D_1 and D_1 are, respectively, given by

$$y_{D_1} = h_{ud_1}(\sqrt{a_1P_r}\hat{x}_1 + \sqrt{a_2P_r}\hat{x}_2) + w_{D_1}, \quad (11)$$

$$y_{D_2} = h_{ud_2}(\sqrt{a_1P_r}\hat{x}_1 + \sqrt{a_2P_r}\hat{x}_2) + w_{D_2}, \quad (12)$$

where $w_{D_i} = \mathcal{CN}(0, \sigma_{D_i}^2)$ is the AWGN at D_i and P_r is the transmit power of the UAV given in (7).

D_2 decodes $\hat{x}_2$ by considering $\hat{x}_1$ as noise, while D_1 first decodes $\hat{x}_2$ and then $\hat{x}_1$. Therefore, the SINR of $\hat{x}_2$ at D_1 is expressed as in (13)

$$\gamma_{D_1}^{\hat{x}_2} = \frac{a_2P_r|h_{ud_1}|^2}{a_1P_r|h_{ud_1}|^2 + \sigma_{D_1}^2}. \quad (13)$$

[4]Since the packet size is M_I (information bits) and the number of channel use is m, the data rate of short packet transmission is $R_s = M_I/m$ in (bit/s/Hz).

After D_1 performs SIC successfully on $\hat{x}_2$, the SINRs of $\hat{x}_1$ at D_1 and $\hat{x}_2$ at D_2 are, respectively, given by

$$\gamma_{D_1}^{\hat{x}_1} = \frac{a_1P_r|h_{ud_1}|^2}{\sigma_{D_1}^2}, \quad (14)$$

$$\gamma_{D_2}^{\hat{x}_2} = \frac{a_2P_r|h_{ud_2}|^2}{a_1P_r|h_{ud_2}|^2 + \sigma_{D_2}^2}. \quad (15)$$

III. PERFORMANCE ANALYSIS

A. BACKGROUNDS ON BLOCKLENGTH ERROR RATE

In conventional channel coding theorem, the error probability of the communication system is often investigated with the infinite blocklength. However, in practice, the system's data rate may be limited due to fixed finite blocklength to ensure target error probability. According to [39], the data rate r_i of finite blocklength m is approximated as[5]

$$r_i(m, \gamma_i, \epsilon_i) \approx C(\gamma_i) - \sqrt{\frac{V(\gamma_i)}{m}}Q^{-1}(\epsilon_i) + O\Big(\frac{\log_2 m}{m}\Big), \quad (16)$$

where $C(\gamma_i) = \log_2(1+\gamma_i)$ is the Shannon capacity, $V(\gamma_i) = (1 - \frac{1}{(1+\gamma_i)^2})(\log_2 e)^2$ refers to the channel dispersion, measured in squared information units per channel use, which represents the variation of channel compared with deterministic channel for the same capacity, ϵ_i is the expected error probability, $Q^{-1}(\cdot)$ is the inverse Gaussian Q-function $Q(x) = \frac{1}{2\pi}\int_x^\infty \exp(-\frac{t^2}{2})dt$, and $O\Big(\frac{\log_2 m}{m}\Big)$ is the remainder term of order $\frac{\log_2 m}{m}$. Since the blocklength[6] is large enough, i.e., $m \ge 100$ as given in [39], from (16), we can rewrite the instantaneous BLER as

$$\epsilon_i \approx Q\left((C(\gamma_i) - r_i)/\sqrt{V(\gamma_i)/m}\right). \quad (17)$$

Let $\phi_{\mathcal{A}}^{x_i}$ be the event that decoding error of x_i occurs at node $\mathcal{A} \in \{UAV, D_1, D_2\}$ and $\bar{\phi}_{\mathcal{A}}^{x_i}$ is the complement of $\phi_{\mathcal{A}}^{x_i}$. From (9) and (10), the instantaneous BLER when decoding x_2 at the UAV is calculated as

$$\Pr(\phi_{AR}^{x_2}) = \epsilon_{AR}^{x_2} \approx Q\Big(\frac{C(\gamma_U^{x_2}) - r_2}{\sqrt{V(\gamma_U^{x_2})/m(1-\kappa)}}\Big), \quad (18)$$

where $\gamma_U^{x_2}$ is given in (9) and $r_2 = 2M/m(1-\kappa)$ with M is the total number of bits of x_2. After the UAV decodes and removes x_2 in (8) successfully, the instantaneous BLER when decoding x_1 at the UAV is

$$\Pr(\phi_{AR}^{x_1}|\bar{\phi}_{AR}^{x_2}) = \epsilon_{AR}^{x_1} \approx Q\Big(\frac{C(\gamma_U^{x_1}) - r_1}{\sqrt{V(\gamma_U^{x_1})/m(1-\kappa)}}\Big), \quad (19)$$

where $\gamma_U^{x_1}$ is given in (10) and $r_1 = 2M/m(1-\kappa)$ with M is the number of bits of user D_1. On the other hand, the

[5]Considering channel coding is out-of-scope of this paper.

[6]The blocklength m of a block code is the number of symbols in a block. Hence, the elements c of a block code is finite and nonempty, which is strings of length m and correspond to blocks. If $c = C(n)$ for a message n, then c is called as the codeword of n.

UAV can decode x_1 in the condition of SIC error at x_2, i.e., $\Pr(\phi_{AR}^{x_1}|\phi_{AR}^{x_2})$. Thus, the probability of error decoding x_1 at the UAV is expressed as

$$\Pr(\phi_{AR}^{x_1}) = \Pr(\phi_{AR}^{x_1}|\phi_{AR}^{x_2})\Pr(\phi_{AR}^{x_2}) + \Pr(\phi_{AR}^{x_1}|\bar{\phi}_{AR}^{x_2})\Pr(\bar{\phi}_{AR}^{x_2}), \tag{20}$$

where $\Pr(\phi_{AR}^{x_1}|\phi_{AR}^{x_2})$ is the conditional probability of $\phi_R^{x_1}$ for a given $\phi_{AR}^{x_2}$. Due to the high interference level from x_2 when decoding x_1, we have $\Pr(\phi_{AR}^{x_1}|\phi_{AR}^{x_2}) \approx 1$. From (20), the total BLER when detecting x_1 at the UAV is calculated as

$$\begin{aligned}\tilde{\epsilon}_{AR}^{x_1} &= 1 \times \epsilon_{AR}^{x_2} + \epsilon_{AR}^{x_1}(1-\epsilon_{AR}^{x_2}) \\ &= \epsilon_{AR}^{x_2} + \epsilon_{AR}^{x_1} - \epsilon_{AR}^{x_1}\epsilon_{AR}^{x_2} \approx \epsilon_{AR}^{x_2} + \epsilon_{AR}^{x_1}.\end{aligned} \tag{21}$$

Note that in (21), the error in URLLC usually small, ranging from 10^{-3} to 10^{-5}. Therefore, the term $\epsilon_{AR}^{x_1}\epsilon_{AR}^{x_2} \to 0$ and can be ignored.

Since the UAV utilizes DF protocol, after receiving the superposed signal, D_2 detects x_2 directly and D_1 applies SIC on x_2 to obtain x_1. Thus, it is assumed that D_i cannot detect x_i if the UAV cannot detect it, i.e., $\Pr(\phi_{D_i}^{x_i}|\phi_{AR}^{x_i}) = 1$. Thus, the BLER when decoding x_1 at D_1 and decoding x_2 at D_2 are, respectively, given by

$$\begin{aligned}\Pr(\phi_{D_1}^{x_1}) &= \tilde{\epsilon}_{AR}^{x_1} + \Pr(\phi_{D_1}^{x_2}) + \Pr(\phi_{D_1}^{x_1}|\bar{\phi}_{D_1}^{x_2})\Pr(\bar{\phi}_{D_1}^{x_2}) \\ &= \tilde{\epsilon}_{AR}^{x_1} + \epsilon_{D_1}^{x_2} + \Pr(\phi_{D_1}^{x_1}|\bar{\phi}_{D_1}^{x_2}).\end{aligned} \tag{22}$$

$$\begin{aligned}\Pr(\phi_{D_2}^{x_2}) &= \Pr(\phi_{D_2}^{x_2}|\phi_{AR}^{x_2})\Pr(\phi_{AR}^{x_2}) + \Pr(\phi_{D_2}^{x_2}|\bar{\phi}_{AR}^{x_2})\Pr(\bar{\phi}_{AR}^{x_2}) \\ &= 1 \times \Pr(\phi_{AR}^{x_2}) + \Pr(\phi_{D_2}^{x_2}|\bar{\phi}_{AR}^{x_2})(1-\Pr(\phi_{AR}^{x_2})).\end{aligned} \tag{23}$$

From (22), the instantaneous BLER of x_1 at D_1 can be calculated as

$$\tilde{\epsilon}_{D_1}^{x_1} = \tilde{\epsilon}_{AR}^{x_1} + \epsilon_{D_1}^{x_2} + \epsilon_{D_1}^{x_1}, \tag{24}$$

and from (23), the instantaneous BLER of x_2 at D_2 can be computed as

$$\tilde{\epsilon}_{D_2}^{x_2} = \epsilon_{AR}^{x_2} + \epsilon_{D_2}^{x_2}(1-\epsilon_{AR}^{x_2}) \approx \epsilon_{AR}^{x_2} + \epsilon_{D_2}^{x_2}, \tag{25}$$

where $\epsilon_{D_1}^{x_2} \approx Q\Big(\frac{(C(\gamma_{D_1}^{\hat{x}_2})-r_2)}{\sqrt{V(\gamma_{D_1}^{\hat{x}_2\to\hat{x}_1})/m(1-\kappa)}}\Big)$, $\epsilon_{D_1}^{x_1} \approx Q\Big(\frac{(C(\gamma_{D_1}^{\hat{x}_1})-r_1)}{\sqrt{V(\gamma_{D_1}^{\hat{x}_1})/m(1-\kappa)}}\Big)$, and $\epsilon_{D_2}^{x_2} \approx Q\Big(\frac{(C(\gamma_{D_2}^{\hat{x}_2})-r_2)}{\sqrt{V(\gamma_{D_2}^{\hat{x}_2})/m(1-\kappa)}}\Big)$, $\tilde{\epsilon}_{AR}^{x_1}$ and $\epsilon_{AR}^{x_2}$ are, respectively, given in (21) and (18).

B. AVERAGE BLER IN FINITE BLOCKLENGTH REGIME

From (17), the average BLER at each node can be presented as

$$\bar{\epsilon}_i \approx \int_0^\infty Q\Big(\frac{C(\gamma_i)-r_i}{\sqrt{V(\gamma_i)/m(1-\kappa)}}\Big) f_{\gamma_i}(x)dx, \tag{26}$$

where $f_{\gamma_i}(x)$ denotes the PDF of the random variable γ_i.

Since it is challenging to derive the exact closed-form expression of (26), we apply the approximate Q-function to solve (26) as similar to [25], [40], [41], and [42], i.e.,

$$Q\Big(\frac{C(\gamma_i)-r_i}{\sqrt{V(\gamma_i)/m}}\Big) = \begin{cases} 1, & \gamma_i \le \rho_L \\ 0.5 - \chi_i(\gamma_i - \tau_i), & \rho_L < \gamma_i < \rho_H, \\ 0, & \gamma_i \ge \rho_H \end{cases} \tag{27}$$

where $\chi_i = [2\pi(2^{2r_i}-1)/m(1-\kappa)]^{-1/2}$, $\tau_i = 2^{r_i}-1$, $\rho_L = \tau_i - 1/(2\chi_i)$, and $\rho_H = \tau_i + 1/(2\chi_i)$.

From (26) and (27), we can rewrite the average BLER as

$$\bar{\epsilon}_i(\Omega_\ell) \approx \chi_i \int_{\rho_L}^{\rho_H} F_{\gamma_i|\Omega_\ell}(x|\Omega_\ell)dx, \tag{28}$$

where $F_{\gamma_i|\Omega_\ell}(x|\Omega_\ell)$ is the conditional CDF of γ_i. To obtain the closed-form of BLER, we first derive $F_{\gamma_i|\Omega_\ell}(x|\Omega_\ell)$, which depends on the SINRs. The CDFs of these SINRs are given in detail in Appendix.

Replacing the CDFs from (47) and (48) into (28), the average BLERs can be given by the following Propositions.

Proposition 1: From (21) and (28), the closed-form expression of the average BLERs of x_1 at the UAV is

$$\begin{aligned}\mathbb{E}\{\tilde{\epsilon}_{AR}^{x_1}\} \approx (&\bar{\epsilon}_{AR,LoS}^{x_2} + \bar{\epsilon}_{AR,LoS}^{x_1})P_{LoS} \\ &+ (\bar{\epsilon}_{AR,NLoS}^{x_2} + \bar{\epsilon}_{AR,NLoS}^{x_1})P_{NLoS},\end{aligned} \tag{29}$$

and from (18), (27) and (28) the closed-form expression of the average BLERs of x_2 at the UAV is

$$\mathbb{E}\{\epsilon_{AR}^{x_2}\} = \bar{\epsilon}_{AR,LoS}^{x_2}P_{LoS} + \bar{\epsilon}_{AR,NLoS}^{x_2}P_{NLoS}, \tag{30}$$

where $\bar{\epsilon}_{AR,LoS}^{x_1}$ and $\bar{\epsilon}_{AR,LoS}^{x_2}$ are, respectively, given in Chebyshev-Gauss approximation[7] as

$$\begin{aligned}\bar{\epsilon}_{AR,LoS}^{x_2} = 1 - \chi_2 &\sum_{l=0}^{L_{max}}\sum_{n=0}^{l}\sum_{\mu=0}^{N}\frac{\pi\beta_{l,n}}{N}\Big(\frac{(K+1)u\sigma_R^2}{\Omega_{su}P_s(a_2-a_1u)}\Big)^n \\ &\times \exp\Big(-\frac{(K+1)u\sigma_R^2}{\Omega_{su}P_s(a_2-a_1u)}\Big)\sqrt{1-\psi^2},\end{aligned} \tag{31}$$

$$\begin{aligned}\bar{\epsilon}_{AR,LoS}^{x_1} = 1 - \chi_1 &\sum_{l=0}^{L_{max}}\sum_{n=0}^{l}\sum_{\mu=0}^{N}\frac{\pi\beta_{l,n}}{N}\Big(\frac{(K+1)u\sigma_R^2}{\Omega_{su}P_sa_1}\Big)^n \\ &\times \exp\Big(-\frac{(K+1)u\sigma_R^2}{\Omega_{su}P_sa_1}\Big)\sqrt{1-\psi^2},\end{aligned} \tag{32}$$

where $u = \frac{\rho_H-\rho_L}{2}\psi + \frac{\rho_H+\rho_L}{2}$, $\psi = cos\Big(\frac{(2\mu-1)\pi}{2N}\Big)$, $L_{max} \in \{1, \infty\}$, and N is the number of terms in Chebyshev-Gauss quadrature. To obtain $\bar{\epsilon}_{AR,NLoS}^{x_i}$, we only replace Ω_ℓ by $\omega\Omega_\ell$ from (5) into (31) and (32). It is also used in [32, Eq. (7)].

To calculate $\bar{\epsilon}_{AR,LoS}^{x_2}$ and $\bar{\epsilon}_{AR,NLoS}^{x_2}$, we replace (47) into (28) and then use the Chebyshev-Gauss approximation. Moreover, we use (48) to calculate $\bar{\epsilon}_{AR,LoS}^{x_1}$. Note that, when calculating the detecting error of x_1 at the UAV, the SIC error of x_2 should be considered, as given in (21).

[7]The Chebyshev-Gauss quadrature is an effective approximation method to calculate the integration of a function $f(x)$ over an interval (a, b), i.e., $\int_a^b f(x)dx \approx \frac{b-a}{2}\sum_{i=1}^{N}\frac{\pi}{N}\sqrt{1-y_i^2}f(x_i)$, where $x_i = \frac{b-a}{2}y_i + \frac{b+a}{2}$, $y_i = \cos(\frac{2i-1}{2N}\pi)$.

Remark 1: Equations (31) and (32) indicate that the BLERs of x_1 and x_2 at the UAV depend on the size $m(1-\kappa)$ of data block over S−UAV link, the average channel gain Ω_{su}, and the power allocation coefficients a_1, a_2. When $u > a_2/a_1$, the upper bound of the BLER of x_2 at the UAV is $\bar{\epsilon}^{x_2}_{R,LoS/NLoS} = 1$.

Proposition 2: From (21) and (24), the closed-form expression of the average BLER at D_1 is

$$\begin{aligned}\mathbb{E}\{\tilde{\epsilon}^{e2e}_{D_1}\} = &(\bar{\epsilon}^{x_2}_{AR,LoS} + \bar{\epsilon}^{x_1}_{AR,LoS} + \bar{\epsilon}^{x_2}_{D_1,LoS} + \bar{\epsilon}^{x_1}_{D_1,LoS})P_{LoS} \\ &+ (\bar{\epsilon}^{x_2}_{AR,NLoS} + \bar{\epsilon}^{x_1}_{AR,NLoS} + \bar{\epsilon}^{x_2}_{D_1,NLoS} \\ &+ \bar{\epsilon}^{x_1}_{D_1,NLoS})P_{NLoS}, \end{aligned} \tag{33}$$

and from (25) the average BLER at D_2 is

$$\begin{aligned}\mathbb{E}\{\tilde{\epsilon}^{e2e}_{D_2}\} \approx &(\bar{\epsilon}^{x_2}_{AR,LoS} + \bar{\epsilon}^{x_2}_{D_2,LoS})P_{LoS} \\ &+ (\bar{\epsilon}^{x_2}_{AR,NLoS} + \bar{\epsilon}^{x_2}_{D_2,NLoS})P_{NLoS}, \end{aligned} \tag{34}$$

where $\bar{\epsilon}^{x_1}_{R,LoS/NLoS}$ and $\bar{\epsilon}^{x_2}_{R,LoS/NLoS}$ are given in Proposition 1. The closed-form expressions of $\bar{\epsilon}^{x_2}_{D_1,LoS}$, $\bar{\epsilon}^{x_1}_{D_1,LoS}$, and $\bar{\epsilon}^{x_2}_{D_2,LoS}$ are given in (35), (36) and (37), as shown at the bottom of next the page, respectively. To obtain $\bar{\epsilon}^{x_2}_{D_1,LoS}$, $\bar{\epsilon}^{x_1}_{D_1,NLoS}$, and $\bar{\epsilon}^{x_2}_{D_2,NLoS}$, we only replace Ω_ℓ by $\omega\Omega_\ell$ from (5) into (35), (36) and (37),

where $\Psi(u) = \frac{u}{a_2 - a_1 u}$, $\Delta = \frac{2\kappa m \xi P_b}{1-\kappa}$, $\beta_{l,n} = \frac{K^l}{l!n!e^K}$, $u = \frac{\rho_H - \rho_L}{2}\psi + \frac{\rho_H + \rho_L}{2}$, $\psi = cos\left(\frac{(2\mu-1)\pi}{2N}\right)$, $L_{max} \in \{1, \infty\}$, and $J_{max} \in \{1, \infty\}$.

To obtain (35), (36), and (37), we replace (57), (59), and (61), as shown at the top of page 13, into (28), respectively, and then do some manipulations. In contrast, after replacing (58), (60) and (62), as shown at the top of page 13, into (28) we obtain $\bar{\epsilon}^{x_2}_{D_1,NLoS}$, $\bar{\epsilon}^{x_1}_{D_1,NLoS}$, and $\bar{\epsilon}^{x_2}_{D_2,NLoS}$, respectively. Note that when considering the BLER at D_i, we must investigate the error at the UAV transferred to D_i.

Remark 2: Equations (33) and (34) show that the BLER at D_i is a function of the transmit power of PB, the average channel gain Ω_{UD_i}, the blocklength $m(1-\kappa)$ over $UAV - D_i$, link. When $u > a_2/a_1$, the upper bounds of the BLERs of x_2 at D_1 and D_2 are, respectively, $\bar{\epsilon}^{x_2}_{D_1,LoS/NLoS} = 1$ and $\bar{\epsilon}^{x_2}_{D_2,LoS/NLoS} = 1$.

C. ASYMPTOTIC EXPRESSION OF THE AVERAGE BLER

For insights into the impacts of system parameters on the BLER performance, we present the asymptotic of the average BLER. As mentioned in [25], the integral in (28) can be approximated by using the first-order Riemann integral, i.e., $\int_a^b f(x)dx = (b-a)f(\frac{a+b}{2})$. Thus, we can rewrite the average BLER as

$$\bar{\epsilon}_i(\Omega_\ell) \approx \chi_i(\rho_H - \rho_L)F_{\gamma_i|\Omega_\ell}\left(\frac{\rho_H + \rho_L}{2}|\Omega_\ell\right), \tag{38}$$

where χ_i, ρ_H, and ρ_L are given in (27). After replacing ρ_H and ρ_L into (38), the BLER can be written as

$$\bar{\epsilon}_i(\Omega_\ell) \approx F_{\gamma_i|\Omega_\ell}(\tau_i|\Omega_\ell), \tag{39}$$

where $\tau_i = 2^{r_i} - 1$. Since τ_i is small enough and a_2 is much larger than a_1, we can present the series of $e^x = \sum_{\mu=0}^{\infty}\frac{(-1)^\mu x^\mu}{\mu!}$ and the approximate of the BLERs at the UAV as

$$\bar{\epsilon}^{x_2}_{AR,LoS} \approx 1 - \sum_{l=0}^{L_{max}}\sum_{n=0}^{l}\sum_{\mu=0}^{N_{max}}\frac{(-1)^\mu \beta_{l,n}\left(\frac{(K+1)\tau_i\sigma_R^2}{\Omega_{su}P_s(a_2 - a_1\tau_i)}\right)^{n+\mu}}{\mu!}, \tag{40}$$

$$\bar{\epsilon}^{x_1}_{AR,LoS} \approx 1 - \sum_{l=0}^{L_{max}}\sum_{n=0}^{l}\sum_{\mu=0}^{N_{max}}\frac{(-1)^\mu \beta_{l,n}}{\mu!}\left(\frac{(K+1)\tau_i\sigma_R^2}{\Omega_{su}P_s a_1}\right)^{n+\mu}. \tag{41}$$

For calculating the BLERs of UAV-D_i link, we replace τ_i by x into the CDFs in (57), (59) and (61). Similar to Proposition 1, we replace Ω_ℓ by $\omega\Omega_\ell$ to obtain the BLER at D_i in NLoS condition.

Remark 3: From (40) and (41), we can get the diversity order at the UAV, $d = \lim_{P_s\to\infty}\frac{\log_2(\bar{\epsilon}^{x_i}_{AR,LoS})}{\log_2(P_s)} = 1$. Moreover, the BLERs at D_i given in (35), (36) and (37) do not depend on P_s. In contrast, since the transmit power of the UAV is harvested from PB, the BLERs at D_i are constants that depend on P_b.

IV. THROUGHPUT ANALYSIS

When the blocklength is very large, the ergodic capacity is always used as an evaluating metric. In contrast, if the blocklength is short, the throughput will be used instead of the ergodic capacity. In this section, we derive the throughput of the investigated NOMA-UAV-SPC system. The throughput of a short-packet communication system is defined as the number of successfully decoded packets per second [39]. Throughput measures the efficiency and effectiveness of the data processing in the considered system. As the block error rate increases, the throughput tends to decrease or vice versa. For a given size $M = M_I + M_e$ bits propagated over m channels with error probability ϵ, the throughput is calculated as [10]

$$\tau^{e2e}_{D_i} = \frac{M - M_e}{M}r_i(1 - \bar{\epsilon}^{e2e}_{D_i}) = \left(1 - \frac{M_e}{M}\right)r_i(1 - \bar{\epsilon}^{e2e}_{D_i}), \tag{42}$$

where M_I is the number of information bits, M_e is the number of training bits, and $\bar{\epsilon}^{e2e}_{D_i}$ is the average BLER given (33) and (34).

For the investigated UAV-NOMA-SPC system, the total throughput is computed as

$$\begin{aligned}\tau(M_e) &= \tau^{e2e}_{D_1} + \tau^{e2e}_{D_2} \\ &= \left(1 - \frac{M_e}{M}\right)\left[r_1(1 - \bar{\epsilon}^{e2e}_{D_1}) + r_2(1 - \bar{\epsilon}^{e2e}_{D_2})\right]. \end{aligned} \tag{43}$$

It is noted that, for a fixed size of information data, increasing M_e will reduce the rate $(M - M_e)/M$, which then improves the system throughput. However, a larger M_e leads to less spectrum efficiency, i.e., the number of information bits is decreased over the same channel uses. On the other hand, reducing the number of information bits, in turn, reduces the throughput. Hence, there is a trade-off between the number

TABLE 3. System parameters used for simulations.

Parameter	Value
H, β_0	5 m $\sim$ 550 m, 20 dB
a_1, a_2, κ, ρ	0.6, 0.4, 0.4, 0.85
$\alpha(\frac{\pi}{2}), \alpha(0), \sigma_U^2, \sigma_{D_i}^2$	2, 3.5, 1 W, 1 W
P_b, v	100 W, 10 m/s

of information bits and the number of training bits that maximizes the system throughput.

V. NUMERICAL RESULTS

In this section, we provide the analytical and simulation results of the average BLER and throughput of the considered NOMA-UAV relay system to evaluate the performance of the investigated system and validate the analytical expressions of BLER and throughput in the previous sections. We use 10×2^{14} independent trials for Monte-Carlo simulations. Since the LoS links dominate the reflection and scattering links, the Rician factor K is integer [43]. Unless otherwise stated, we let the number of transmitted bits $M = 256$ and $M = 128$, the packet length $m = 200$. The locations of all nodes are set as follows: $S(-300, 0, 0)$, $PB(-100, -100, 0)$, $D_1(200, 0, 0)$, $D_2(250, 100, 0)$, the starting location of the UAV is $q_I = (-200, 0, 150)$ and the ending location of the UAV is $q_F = (200, 0, 150)$. The coefficients for different urban environments are given in Table 2. Unless otherwise indicated in the figures, parameter settings are presented in Table 3. For achieving the BLERs threshold of the system, we set SNR = 30 dB [14], [22] and the UAV velocity $v = 10$ m/s.

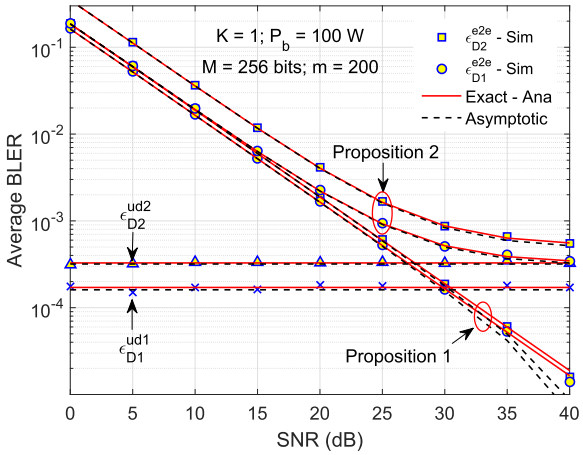

FIGURE 2. Average BLERs of x_1 and x_2 at the UAV and D_1 and D_2 versus the SNR; $K = 1$, $\omega = 0.7$, and $m = 200$.

Fig. 2 plots the average BLERs of x_1 and x_2 at the UAV using Proposition 1 and the average BLERs of x_1 and x_2 at D_1 and D_2 using Proposition 2. Moreover, the BLERs of UAV–D_1 and UAV–D_2 channels are also given. As observed from Fig. 2, the BLERs of UAV–D_1 and UAV–D_2 channels do not change with the SNR because the transmit power at the UAV is fixed. In contrast, the BLERs of x_1 and x_2 at the UAV decrease with the increase of the SNR. In contrast, the BLERs of the average BLERs of x_1 and x_2 at D_1 and D_2 (Proposition 2) are first decreased as the SNR increases and then are saturated as the SNR becomes higher. This feature is because the errors of the first hop are transferred to the second hop, i.e., the end-to-end BLERs are the cumulative

$$\bar{\epsilon}_{D_1,LoS}^{x_2} = 1 - \chi_2 \sum_{l=0}^{L_{max}} \sum_{n=0}^{l} \sum_{j=0}^{J_{max}} \frac{\beta_{l,n}}{(j!)^2} \left(\frac{K(K+1)}{\Omega_{bu}}\right)^j \frac{K+1}{\Omega_{bu} e^K} \sum_{\mu=0}^{N} \frac{\pi}{N} \left(\frac{(K+1)\sigma_{D_1}^2 \Psi(u)}{\Delta\Omega_{ud_1}}\right)^n \times 2\left(\frac{\sigma_{D_1}^2 \Omega_{bu}}{\Delta\Omega_{ud_1}} \Psi(u)\right)^{\frac{j-n+1}{2}} \mathcal{K}_{j-n+1}\left(2\sqrt{\frac{(K+1)^2 \Psi(u) \sigma_{D_1}^2}{\Delta\Omega_{ud_1}\Omega_{bu}}}\right) e^{-\frac{(K+1)\sigma_{D_1}^2 \Psi(u)}{\Delta\Omega_{ud_1}}} \sqrt{1-\psi^2}, . \quad (35)$$

$$\bar{\epsilon}_{D_1,LoS}^{x_1} = 1 - \chi_1 \sum_{l=0}^{L_{max}} \sum_{n=0}^{l} \sum_{j=0}^{J_{max}} \frac{\beta_{l,n}}{(j!)^2} \left(\frac{K(K+1)}{\Omega_{bu}}\right)^j \frac{K+1}{\Omega_{bu} e^K} \sum_{\mu=0}^{N} \frac{\pi}{N} \left(\frac{(K+1)u\sigma_{D_1}^2}{\Delta\Omega_{ud_1} a_1}\right)^n e^{-\frac{(K+1)u\sigma_{D_1}^2}{\Delta\Omega_{ud_1} a_1}} \times 2\left(\frac{u\sigma_{D_1}^2 \Omega_{bu}}{\Delta\Omega_{ud_1} a_1}\right)^{\frac{j-n+1}{2}} \mathcal{K}_{j-n+1}\left(2\sqrt{\frac{(K+1)^2 u\sigma_{D_1}^2}{\Delta\Omega_{ud_1}\Omega_{bu} a_1}}\right) \sqrt{1-\psi^2}, \quad (36)$$

$$\bar{\epsilon}_{D_2,LoS}^{x_2} = 1 - \chi_2 \sum_{l=0}^{L_{max}} \sum_{n=0}^{l} \sum_{j=0}^{J_{max}} \frac{\beta_{l,n}}{(j!)^2} \left(\frac{K(K+1)}{\Omega_{bu}}\right)^j \frac{K+1}{\Omega_{bu} e^K} \sum_{\mu=0}^{N} \frac{\pi}{N} \left(\frac{(K+1)\sigma_{D_2}^2}{\Delta\Omega_{ud_2}} \Psi(u)\right)^n \times 2\left(\frac{\sigma_{D_2}^2 \Omega_{bu}}{\Delta\Omega_{ud_2}} \Psi(u)\right)^{\frac{j-n+1}{2}} \mathcal{K}_{j-n+1}\left(2\sqrt{\frac{(K+1)^2 \sigma_{D_2}^2}{\Delta\Omega_{ud_2}\Omega_{bu}} \Psi(u)}\right) e^{-\frac{(K+1)\sigma_{D_2}^2}{\Delta\Omega_{ud_2}} \Psi(u)} \sqrt{1-\psi^2}, \quad (37)$$

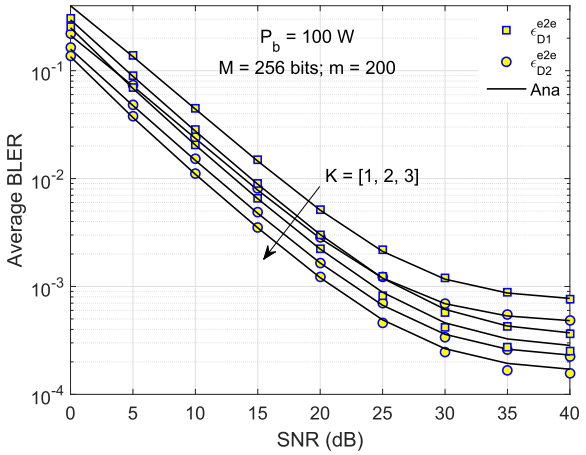

FIGURE 3. Average BLERs of x_1 and x_2 at D_1 and D_2 versus the SNR for different K; $\omega = 0.7$, $m = 200$, urban environment.

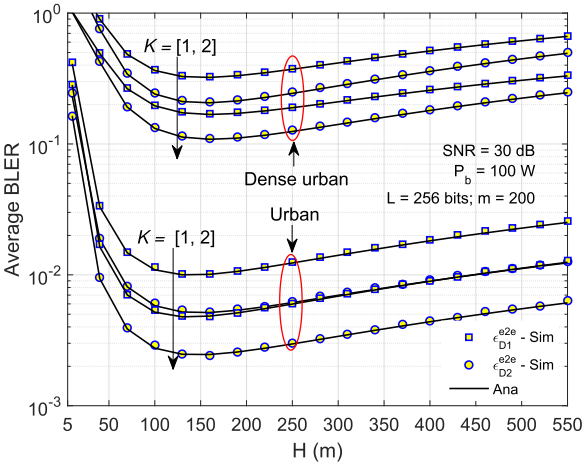

FIGURE 4. Average BLERs of x_1 and x_2 at D_1 and D_2 versus the UAV's altitude H for different urban environments; $K = 1$, $\omega = 0.7$, and $m = 200$.

errors at UAV and D_i. In addition, the error of x_1 at D_1 is lower than that of x_2 at D_2 because D_1 detects x_1 after performing SIC on x_2, i.e., without interference, while D_2 detects x_2 by considering x_1 as the interference. Finally, the approximate and simulation results closely match the exact ones.

Fig. 3 demonstrates the average BLER of x_1 and x_2 at D_1 and D_2 versus the SNR for different values of Rice factor K. Firstly, we can see that the average BLERs decrease when K increases because increasing K makes the LoS probabilities higher. Secondly, these average BLERs linearly reduce when SNR $<$ 25 dB, and then the floor in the high SNR regime. The reason behind this feature is that there always exist interferences among signals in power-domain NOMA systems that limit the system performance. Similar behaviors were also mentioned in [3] and [8]. Moreover, the BLER of x_1 at D_1 is lower than that of x_2 at D_2 because the duration for detecting x_1 only takes one time slot.

Fig. 4 shows the average BLERs of x_1 and x_2 at D_1 and D_2 versus the altitude H of the UAV for different urban environments and Rice factor K with SNR $=$ 30 dB, $P_b =$ 100 W, packet size $M = 256$ bits, and blocklength $m = 200$.

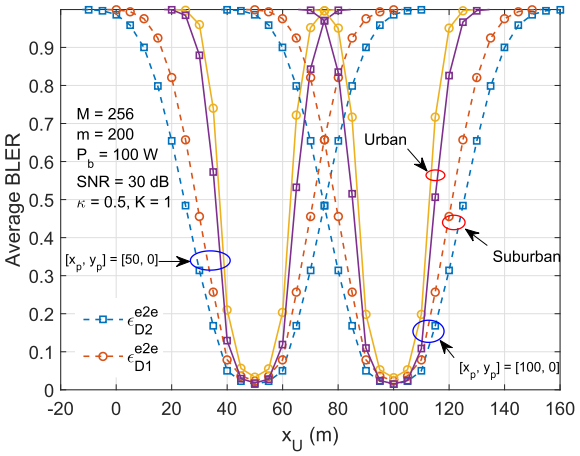

FIGURE 5. Average BLERs of x_1 and x_2 at D_1 and D_2 versus x_U for different urban environments and locations of PB; $K = 1$, $M = 256$, $m = 200$, and $\omega = 0.7$.

When the altitude of the UAV is low (i.e., $H = 5$ m), the path-loss is high because the signal propagation on the ground is affected by severe blockages, $\alpha(0) = 3.5$, and $P_{Los}(0) \to 0$. When H increases, the BLERs decrease to the minimum value and then increase. It implies that there are the optimal altitudes of the UAV that provide the lowest BLERs. We observe that these minimum values are different and depend on the urban environments. The reason behind this feature is that when the altitude of the UAV becomes higher, the LoS probability is also higher, which in turn improves the channel gain. In contrast, a higher UAV's altitude makes the communication link longer, resulting in higher path loss. On the other hand, the error at D_1 is higher than that at D_2 because the SIC technique is applied at D_1, providing interference-free at D_1. Finally, the urban environment gives similar BLERs as dense urban.

Fig. 5 depicts the average BLERs of x_1 and x_2 at D_1 and D_2 versus the location of the UAV for different environments and locations of PB. As shown in Fig. 5, since the path-loss of the urban environment is higher than that of the suburban environment, the urban environment has worse BLER performance. On the other hand, the BLER of x_2 at D_2 is lower than that of x_1 at D_1. It is because the detecting error of x_2 impacts the BLER of x_1 at D_1, and the error at the UAV is transferred to D_1. Moreover, the location of PB greatly influences the minimal BLERs. Particularly, for $[x_p, y_p] = [50, 0]$, the minimal BLER occurs at $x_U = 50$ (m), while $[x_p, y_p] = [100, 0]$, the minimal BLER happens at $x_U = 100$ (m). It means the best BLER performance is achieved when the UAV is right above the PB, which is reasonable because the distance between the PB and the UAV is shortest, leading to the highest amount of harvested energy. Moreover, there exists a location of the UAV that gives the best BLER performance.

Fig. 6 presents the average BLERs of x_1 and x_2 at D_1 and D_2 versus the blocklength (the channel utilization) m with the fixed number of training bits and information bits. For

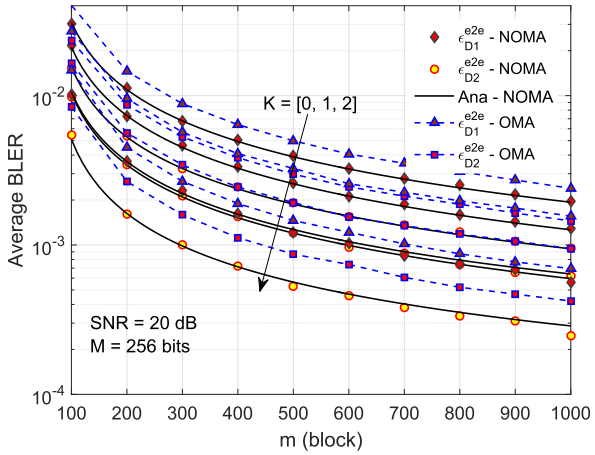

FIGURE 6. Average BLERs of x_1 and x_2 at D_1 and D_2 versus the blocklength m for different K; $M = 256$ and $\omega = 0.7$.

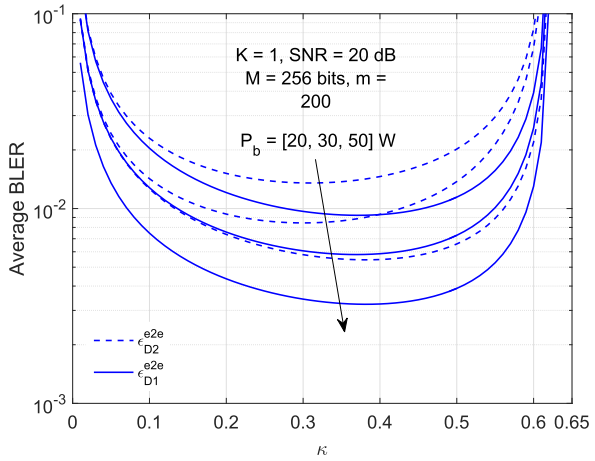

FIGURE 7. Average BLERs of x_1 and x_2 at D_1 and D_2 versus the time switching ratio κ for different transmit power of PB, $M = 256$, $K = 1$, $m = 200$, and SNR = 20 dB.

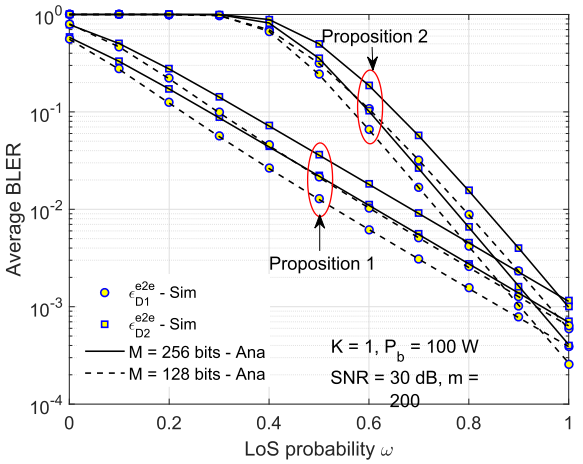

FIGURE 8. Average BLERs of x_1 and x_2 D_1 and D_2 versus LoS probability in urban environment for different packet sizes; SNR = 30 dB, $K = 1$.

comparison, we also give the BLER of the UAV-OMA-SPC system. From Fig. 6, we see that the BLERs are reduced as the blocklength gets larger. It means that, for a fixed number of transmitted information bits, increasing the number of channel utilization, i.e., reducing the number of bits propagating over the channel, results in improved BLER performance. However, it may reduce the spectrum efficiency. Furthermore, increasing K means the LoS channel gain is higher, thus improving BLER performance. Note that when $K = 0$, the channel fading follows the Rayleigh distribution. On the other hand, the BLER of the UAV-NOMA-SPC system is better than that of the UAV-OMA-SPC system because the system performance is linearly proportional to the bandwidth usage.

Fig. 7 shows the average BLERs of x_1 and x_2 at D_1 and D_2 versus the switching ratio κ for different transmit power of PB. From Fig. 7, we see that there exists the optimal values κ_{opt} of κ, which minimizes the average BLERs. Moreover, different κ_{opt} minimal BLERs can be achieved for different transmit power of PB. On the other hand, the BLER performance of x_1 at D_1 is lower than that of x_2 at D_2. In addition, the energy harvesting time must be appropriately determined to ensure enough time for signal processing. Moreover, larger κ means the transmit power of PB is higher, i.e., the signal processing time is shorter. In other words, the signal processing time can be reduced for a fixed error threshold when the transmit power is higher.

Fig. 8 illustrates the average BLERs of x_1 and x_2 at the UAV, D_1, and D_2 versus the LoS probability for different packet sizes, SNR $=$ 30 dB and $m = 200$. Note that only the channels used for actual data transmission are considered; thus, the number of used channels for training is out of the scope. As shown in Fig. 8, the BLERs decrease as the LoS probability increases. Moreover, when $\omega = 1$, the system achieves ideal transmission as free-space communication, and when $\omega = 0$, BLERs are almost equal to one. On the other hand, the BLERs of x_1 are lower than those of x_2 because the interference from x_1 impacts the signal detection of x_2. Additionally, for the same number of used channels, the BLERs in the case of a small number of transmitted bits (i.e., $M = 128$) is better than in the case of a large number of transmitted bits (i.e., $M = 256$).

Fig. 9 plots the throughput of D_i and the whole system versus the SNR in dB for different velocities of the UAV. From Fig. 9, we see that the throughput of x_1 is higher than that of x_2, which means the possibility of successfully detecting x_1 is higher. It is because x_2 is detected by considering x_1 as interference, while x_1 is detected after successfully performing SIC on x_2. On the other hand, the velocity of the UAV significantly affects the achieved throughput. Specifically the throughput when the UAV is stationary ($v = 0$) is better than the throughput when $v = 20$, i.e., $\tau = 12$ bit/s/Hz versus $\tau = 8$ bit/s/Hz. Moreover, the throughput is saturated in the high SNR region (i.e., SNR $>$ 20 dB), confirming Remark 3, i.e., the system performance is constrained by the transmit power of PB.

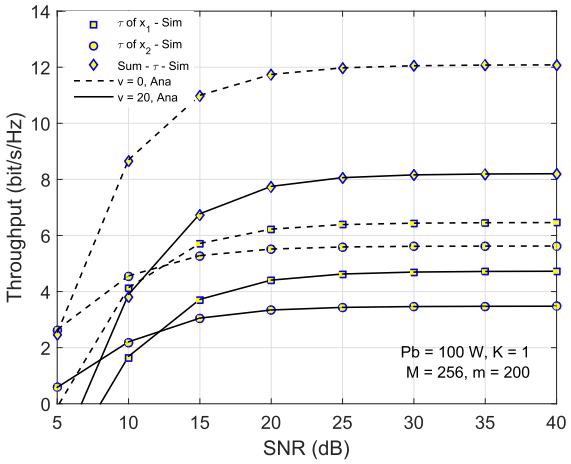

FIGURE 9. Throughput of D_i and the whole system versus the SNR different velocities v of the UAV; $M = 256$, $m = 200$.

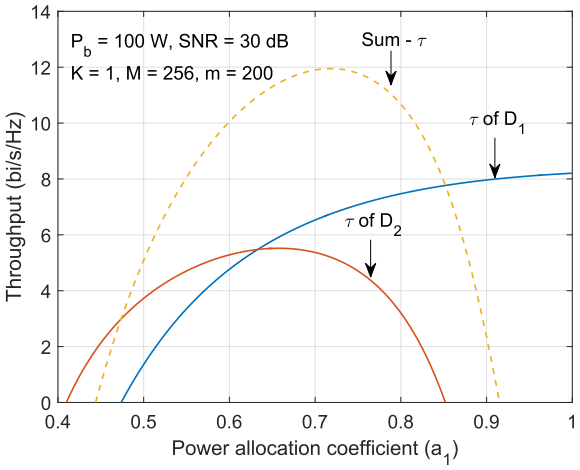

FIGURE 11. Throughput of D_i and whole system versus the power allocation coefficient (a_1); SNR = 30 dB, $M = 256$, $m = 200$, $r = 4$.

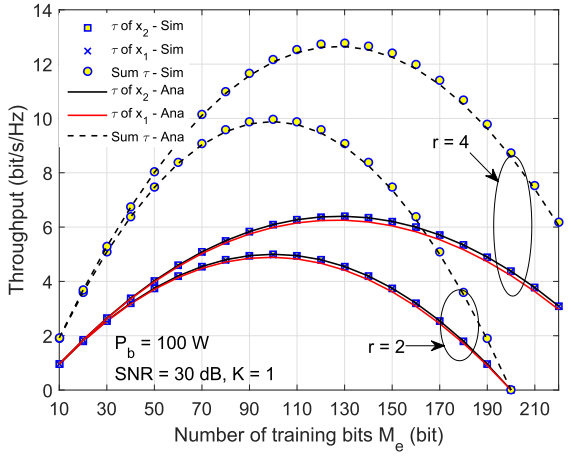

FIGURE 10. Throughput of D_i and whole system versus the number of training bits for different data rates; SNR = 30 dB, $M = 256$.

Fig. 10 depicts the throughput of D_i and the whole system versus the number of training bits for different data rates. As observed in Fig.10, higher data rate r leads to better throughput for the same number of training bits M_e. In addition, a higher data rate needs more training bits, i.e., for the case $r = 2$, the maximal throughput is obtained at 80 training bits, while for the case $r = 4$, nearly 130 training bits are needed to achieve the maximal throughput. Moreover, the throughputs increase with M_e to the maximal values and then decrease as M_e increases further. It is because for a given bit stream, increasing the number of training bits reduces the number of information bits, i.e., lower throughput. On the other hand, lowering the number of training bits increases the decoding error, i.e., lower system throughput. Furthermore, the analysis results are consistent with the simulation results, confirming the correctness of the mathematical analysis.

Fig. 11 depicts the throughputs versus the power allocation for D_1, i.e., a_1 for fixed transmit power SNR = 30 dB and data rate $r = 4$. It is noted that the power allocation for D_2 is $a_2 = 1 - a_1$. When the power allocation coefficient a_1 increases from 0.4 to 1, the sum throughput and throughput of D_2 increase, reach the maximal value, and then reduce. Meanwhile, the throughput of D_1 continuously increases. It is because higher a_1 (or lower a_2) means more power is allocated to D_1, leading to higher throughput. On the other hand, we also see that the optimal system throughput is obtained at $a_1 = 0.7$ and the balanced throughputs of D_1 and D_2 are achieved at $a_1 \approx 0.63$.

VI. CONCLUSION

In this paper, we have analyzed the performance of the UAV-assisted NOMA relay system for SPC, where the UAV harvested energy from a power beacon to support the transmissions of finite blocklength packets from a source to two destinations. The system performance in terms of BLER and throughput over Rician fading channels was investigated. Based on the approximate Chebyshev-Gauss quadrature and the first-order Riemann integral, we obtained the closed-form expressions of the BLERs of each hop and the whole path. Simulation results verified all analytical results. The results indicated that the optimal altitude of the UAV is $H \approx 100$ m provided the best system BLERs. Moreover, the time switching ratio energy harvesting $\kappa = 0.35$ gave the smallest BLER. The number of training bits was chosen in the range $80 < M_e < 130$ to maximize the throughput. The BLER of the UAV-NOMA-SPC was compared with that of the UAV-OMA-SPC systems, indicating that the UAV-NOMA-SPC had lower BLERs. The considered system is suitable for narrow-band systems in the cases the infrastructure systems cannot be deployed, is overloaded, or broken. The considered system can be applied to various IoT applications. For example, in a smart traffic system, D_1 can be a remote-control car receiving control messages that usually contain a few bytes but are time-critical. At the same time, D_2 can be

a self-driving car receiving the confidential driving routes from S. Moreover, the considered system model can be used for an artillery targeting center controlling many artillery units through a UAV.

APPENDIX

This appendix provides step-by-step derivations to obtain the CDF of the SINR at each node with the Rician fading channel. Since X has Rician distribution, after applying the first-order Marcum Q-function, we have

$$F_X(x) = 1 - Q_1(\sqrt{2K}, \sqrt{2\beta_i x}), \tag{44}$$

where $\beta_i = \frac{K+1}{\Omega_i}$ with $\Omega_i = \mathbb{E}\{X\}$ is the expected value of X. Using [43, Eq. (4.18)] and changing the zero-order modified Bessel function into the series formulas, we obtain $F_X(x)$ and $f_X(x)$ as

$$F_X(x) = 1 - \sum_{l=0}^{\infty}\sum_{n=0}^{l} \beta_{l,n}(\beta_i x_i)^n \exp(-\beta_i x_i), \tag{45}$$

$$[3pt] f_X(x) = \frac{\beta_i}{e^K}\exp(-\beta_i x)\sum_{j=0}^{\infty}\frac{1}{(j!)^2}\Big(\frac{K(K+1)x}{\Omega_i}\Big)^j, \tag{46}$$

where $\beta_{l,n} = \frac{K^l}{l!n!e^K}$.

From (5), (9), and (10), we have $F_{\gamma_U^{x_1}}(x)$ and $F_{\gamma_U^{x_2}}(x)$ as

$$F_{\gamma_U^{x_2}}(x) = P_{LoS}\underbrace{\Pr\Big(|h_{su}|^2 < \frac{x\sigma_R^2}{P_s(a_2 - a_1 x)}|_{\omega=1}\Big)}_{\mathcal{I}_1} + P_{NLoS}\underbrace{\Pr\Big(|h_{su}|^2 < \frac{x\sigma_R^2}{P_s(a_2 - a_1 x)}|_{\omega<1}\Big)}_{\mathcal{I}_2}, \tag{47}$$

$$F_{\gamma_U^{x_1}}(x) = P_{LoS}\underbrace{\Pr\Big(|h_{su}|^2 < \frac{x\sigma_R^2}{a_1 P_s}|_{\omega=1}\Big)}_{\mathcal{I}_3} + P_{NLoS}\underbrace{\Pr\Big(|h_{su}|^2 < \frac{x\sigma_R^2}{a_1 P_s}|_{\omega<1}\Big)}_{\mathcal{I}_4}. \tag{48}$$

Applying (45) for (47) and (48), we have the CDFs of the SNRs of x_1 and x_2 at the UAV in the cases of LoS and NLoS communications and with the average power gain Ω_ℓ given in (5) as

$$\mathcal{I}_1 = 1 - \sum_{l=0}^{\infty}\sum_{n=0}^{l}\beta_{l,n}\Big(\frac{(K+1)x\sigma_R^2}{\Omega_{su}P_s(a_2 - a_1 x)}\Big)^n e^{-\frac{(K+1)x\sigma_R^2}{\Omega_{su}P_s(a_2-a_1x)}}, \tag{49}$$

$$\mathcal{I}_2 = 1 - \sum_{l=0}^{\infty}\sum_{n=0}^{l}\beta_{l,n}\Big(\frac{(K+1)x\sigma_R^2}{\omega\Omega_{su}P_s(a_2 - a_1 x)}\Big)^n e^{-\frac{(K+1)x\sigma_R^2}{\omega\Omega_{su}P_s(a_2-a_1x)}}, \tag{50}$$

$$\mathcal{I}_3 = 1 - \sum_{l=0}^{\infty}\sum_{n=0}^{l}\beta_{l,n}\Big(\frac{(K+1)x\sigma_R^2}{\Omega_{su}P_s a_1}\Big)^n e^{-\frac{(K+1)x\sigma_R^2}{\Omega_{su}P_s a_1}}, \tag{51}$$

$$\mathcal{I}_4 = 1 - \sum_{l=0}^{\infty}\sum_{n=0}^{l}\beta_{l,n}\Big(\frac{(K+1)x\sigma_R^2}{\omega\Omega_{su}P_s a_1}\Big)^n e^{-\frac{(K+1)x\sigma_R^2}{\omega\Omega_{su}P_s a_1}}. \tag{52}$$

Next, we calculate the CDFs for $\gamma_{D_1}^{\hat{x}_2}$, $\gamma_{D_1}^{\hat{x}_1}$ and $\gamma_{D_2}^{\hat{x}_2}$ given in (13), (14), and (15), respectively. From (13), we can rewrite the CDF of $\gamma_{D_1}^{\hat{x}_2}$ as

$$F_{\gamma_{D_1}^{\hat{x}_2}}(x) = P_{LoS}\underbrace{\Pr\Big(|h_{pu}|^2|h_{ud_1}|^2 < \frac{x\sigma_{D_1}^2}{\Delta(a_2 - a_1 x)}|_{\omega=1}\Big)}_{\mathcal{I}_5} + P_{NLoS}\underbrace{\Pr\Big(|h_{pu}|^2|h_{ud_1}|^2 < \frac{x\sigma_{D_1}^2}{\Delta(a_2 - a_1 x)}|_{\omega<1}\Big)}_{\mathcal{I}_6}, \tag{53}$$

where Δ is presented in (7).

From (14) and (15), we have the CDF of $\gamma_{D_1}^{\hat{x}_1}$ and the CDF of $\gamma_{D_2}^{\hat{x}_2}$ in the case of perfect SIC as

$$F_{\gamma_{D_1}}^{\hat{x}_1}(x) = P_{LoS}\underbrace{\Pr\Big(|h_{pu}|^2|h_{ud_1}|^2 < \frac{x\sigma_{D_1}^2}{\Delta a_1}|\omega = 1\Big)}_{\mathcal{I}_7} + P_{NLoS}\underbrace{\Pr\Big(|h_{pu}|^2|h_{ud_1}|^2 < \frac{x\sigma_{D_1}^2}{\Delta a_1}|\omega < 1\Big)}_{\mathcal{I}_8}, \tag{54}$$

$$F_{\gamma_{D_2}^{\hat{x}_2}}(x) = P_{LoS}\underbrace{\Pr\Big(|h_{pu}|^2|h_{ud_2}|^2 < \frac{x\sigma_{D_2}^2}{\Delta(a_2 - a_1 x)}|_{\omega=1}\Big)}_{\mathcal{I}_9} + P_{NLoS}\underbrace{\Pr\Big(|h_{pu}|^2|h_{ud_2}|^2 < \frac{x\sigma_{D_2}^2}{\Delta(a_2 - a_1 x)}|_{\omega<1}\Big)}_{\mathcal{I}_{10}}. \tag{55}$$

Thanks to the fundamental of the conditional probability given in [44, Chapter 4], we can rewrite $\mathcal{I}_5$ as

$$\mathcal{I}_5 = \int_0^{\infty} F_{|h_{ud_1}|^2}\Big(\frac{x\sigma_{D_1}^2}{y\Delta(a_2 - a_1 x)}\Big) f_{|h_{pu}|^2}(y)dy. \tag{56}$$

Substituting (45) and (46) into (56), and then using [45, Eq. (3. 471[9])], we obtain the closed-form of $\mathcal{I}_5$ in the case of LoS communication as in (57). Plugging Ω_{bu} and Ω_{ud_1} by $\omega\Omega_{bu}$ and $\omega\Omega_{ud_1}$ into (57) we get $\mathcal{I}_6$ as in (58). These expressions are shown at the top of the next page. Similar to calculating for (53), we can derive the CDFs of $\gamma_{D_1}{}^{\hat{x}_1}$ and $\gamma_{D_2}^{\hat{x}_2}$ for (54) and (55).

$$\mathcal{I}_5 = 1 - \sum_{l=0}^{\infty}\sum_{n=0}^{l}\sum_{j=0}^{\infty} \frac{\beta_{l,n}}{(j!)^2}\Big(\frac{K(K+1)}{\Omega_{bu}}\Big)^j \frac{K+1}{\Omega_{bu}e^K}\Big(\frac{(K+1)x\sigma_{D_1}^2}{\Delta\Omega_{ud_1}(a_2-a_1x)}\Big)^n e^{-\frac{(K+1)x\sigma_{D_1}^2}{\Delta\Omega_{ud_1}(a_2-a_1x)}}$$
$$\times\, 2\Big(\frac{x\sigma_{D_1}^2\Omega_{bu}}{\Delta\Omega_{ud_1}(a_2-a_1x)}\Big)^{\frac{j-n+1}{2}} \mathcal{K}_{j-n+1}\Big(2\sqrt{\frac{(K+1)x\sigma_{D_1}^2}{\Delta\Omega_{ud_1}(a_2-a_1x)}\frac{K+1}{\Omega_{bu}}}\Big), \quad \beta_{l,n} = \frac{K^l}{l!n!e^K}, \tag{57}$$

$$\mathcal{I}_6 = 1 - \sum_{l=0}^{\infty}\sum_{n=0}^{l}\sum_{j=0}^{\infty} \frac{\beta_{l,n}}{(j!)^2}\Big(\frac{K(K+1)}{\omega\Omega_{bu}}\Big)^j \frac{K+1}{\omega\Omega_{bu}e^K}\Big(\frac{(K+1)x\sigma_{D_1}^2}{\Delta\omega\Omega_{ud_1}(a_2-a_1x)}\Big)^n e^{-\frac{(K+1)x\sigma_{D_1}^2}{\Delta\omega\Omega_{ud_1}(a_2-a_1x)}}$$
$$\times\, 2\Big(\frac{x\sigma_{D_1}^2\omega\Omega_{bu}}{\Delta\omega\Omega_{ud_1}(a_2-a_1x)}\Big)^{\frac{j-n+1}{2}} \mathcal{K}_{j-n+1}\Big(2\sqrt{\frac{(K+1)x\sigma_{D_1}^2}{\Delta\omega\Omega_{ud_1}(a_2-a_1x)}\frac{K+1}{\omega\Omega_{bu}}}\Big). \tag{58}$$

$$\mathcal{I}_7 = 1 - \sum_{l=0}^{\infty}\sum_{n=0}^{l}\sum_{j=0}^{\infty} \frac{\beta_{l,n}}{(j!)^2}\Big(\frac{K(K+1)}{\Omega_{bu}}\Big)^j \frac{K+1}{\Omega_{bu}e^K}\Big(\frac{(K+1)x\sigma_{D_1}^2}{\Delta\Omega_{ud_1}a_1}\Big)^n \exp\Big(-\frac{(K+1)x\sigma_{D_1}^2}{\Delta\Omega_{ud_1}a_1}\Big)$$
$$\times\, 2\Big(\frac{x\sigma_{D_1}^2\Omega_{bu}}{\Delta\Omega_{ud_1}a_1}\Big)^{\frac{j-n+1}{2}} \mathcal{K}_{j-n+1}\Big(2\sqrt{\frac{(K+1)x\sigma_{D_1}^2}{\Delta\Omega_{ud_1}a_1}\frac{K+1}{\Omega_{bu}}}\Big), \tag{59}$$

$$\mathcal{I}_8 = 1 - \sum_{l=0}^{\infty}\sum_{n=0}^{l}\sum_{j=0}^{\infty} \frac{\beta_{l,n}}{(j!)^2}\Big(\frac{K(K+1)}{\omega\Omega_{bu}}\Big)^j \frac{K+1}{\omega\Omega_{bu}e^K}\Big(\frac{(K+1)x\sigma_{D_1}^2}{\Delta\omega\Omega_{ud_1}a_1}\Big)^n \exp\Big(-\frac{(K+1)x\sigma_{D_1}^2}{\Delta\omega\Omega_{ud_1}a_1}\Big)$$
$$\times\, 2\Big(\frac{x\sigma_{D_1}^2\omega\Omega_{bu}}{\Delta\omega\Omega_{ud_1}a_1}\Big)^{\frac{j-n+1}{2}} \mathcal{K}_{j-n+1}\Big(2\sqrt{\frac{(K+1)x\sigma_{D_1}^2}{\Delta\omega\Omega_{ud_1}a_1}\frac{K+1}{\omega\Omega_{bu}}}\Big). \tag{60}$$

$$\mathcal{I}_9 = 1 - \sum_{l=0}^{\infty}\sum_{n=0}^{l}\sum_{j=0}^{\infty} \frac{\beta_{l,n}}{(j!)^2}\Big(\frac{K(K+1)}{\Omega_{bu}}\Big)^j \frac{K+1}{\Omega_{bu}e^K}\Big(\frac{(K+1)x\sigma_{D_2}^2}{\Delta\Omega_{ud_2}(a_2-a_1x)}\Big)^n e^{-\frac{(K+1)x\sigma_{D_2}^2}{\Delta\Omega_{ud_2}(a_2-a_1x)}}$$
$$\times\, 2\Big(\frac{x\sigma_{D_2}^2\Omega_{bu}}{\Delta\Omega_{ud_2}(a_2-a_1x)}\Big)^{\frac{j-n+1}{2}} \mathcal{K}_{j-n+1}\Big(2\sqrt{\frac{(K+1)x\sigma_{D_2}^2}{\Delta\Omega_{ud_2}(a_2-a_1x)}\frac{K+1}{\Omega_{bu}}}\Big), \tag{61}$$

$$\mathcal{I}_{10} = 1 - \sum_{l=0}^{\infty}\sum_{n=0}^{l}\sum_{j=0}^{\infty} \frac{\beta_{l,n}}{(j!)^2}\Big(\frac{K(K+1)}{\omega\Omega_{bu}}\Big)^j \frac{K+1}{\omega\Omega_{bu}e^K}\Big(\frac{(K+1)x\sigma_{D_2}^2}{\Delta\omega\Omega_{ud_2}(a_2-a_1x)}\Big)^n e^{-\frac{(K+1)x\sigma_{D_2}^2}{\Delta\omega\Omega_{ud_2}(a_2-a_1x)}}$$
$$\times\, 2\Big(\frac{x\sigma_{D_2}^2\omega\Omega_{bu}}{\Delta\omega\Omega_{ud_2}(a_2-a_1x)}\Big)^{\frac{j-n+1}{2}} \mathcal{K}_{j-n+1}\Big(2\sqrt{\frac{(K+1)x\sigma_{D_2}^2}{\Delta\omega\Omega_{ud_2}(a_2-a_1x)}\frac{K+1}{\omega\Omega_{bu}}}\Big) \tag{62}$$

REFERENCES

[1] M. Mozaffari, X. Lin, and S. Hayes, "Toward 6G with connected sky: UAVs and beyond," *IEEE Commun. Mag.*, vol. 59, no. 12, pp. 74–80, Dec. 2021.

[2] M. E. Tanab and W. Hamouda, "Efficient resource allocation in fast-uplink grant for machine-type communications with NOMA," *IEEE Internet Things J.*, vol. 9, no. 18, pp. 18113–18129, Sep. 2022, doi: 10.1109/JIOT.2022.3163190.

[3] T. M. Hoang, L. T. Dung, B. C. Nguyen, X. N. Tran, and T. Kim, "Secrecy outage performance of FD-NOMA relay system with multiple non-colluding eavesdroppers," *IEEE Trans. Veh. Technol.*, vol. 70, no. 12, pp. 12985–12997, Dec. 2021.

[4] A. Ranjha and G. Kaddoum, "URLLC-enabled by laser powered UAV relay: A quasi-optimal design of resource allocation, trajectory planning and energy harvesting," *IEEE Trans. Veh. Technol.*, vol. 71, no. 1, pp. 753–765, Jan. 2022.

[5] W. Wang, X. Li, R. Wang, K. Cumanan, W. Feng, Z. Ding, and O. A. Dobre, "Robust 3D-trajectory and time switching optimization for dual-UAV-enabled secure communications," *IEEE J. Sel. Areas Commun.*, vol. 39, no. 11, pp. 3334–3347, Nov. 2021.

[6] M. Huang, A. Liu, N. N. Xiong, and J. Wu, "A UAV-assisted ubiquitous trust communication system in 5G and beyond networks," *IEEE J. Sel. Areas Commun.*, vol. 39, no. 11, pp. 3444–3458, Nov. 2021.

[7] Y. Wang, W. Feng, J. Wang, and T. Q. S. Quek, "Hybrid satellite-UAV-terrestrial networks for 6G ubiquitous coverage: A maritime communications perspective," *IEEE J. Sel. Areas Commun.*, vol. 39, no. 11, pp. 3475–3490, Nov. 2021.

[8] T. M. Hoang, B. C. Nguyen, L. T. Dung, and T. Kim, "Outage performance of multi-antenna mobile UAV-assisted NOMA relay systems over Nakagami-*m* fading channels," *IEEE Access*, vol. 8, pp. 215033–215043, 2020.

[9] P. Raut, K. Singh, C.-P. Li, M.-S. Alouini, and W.-J. Huang, "Nonlinear EH-based UAV-assisted FD IoT networks: Infinite and finite blocklength analysis," *IEEE Internet Things J.*, vol. 8, no. 24, pp. 655–668, Dec. 2021.

[10] N. Agrawal, A. Bansal, K. Singh, C.-P. Li, and S. Mumtaz, "Finite block length analysis of RIS-assisted UAV-based multiuser IoT communication system with non-linear EH," *IEEE Trans. Commun.*, vol. 70, no. 5, pp. 3542–3557, May 2022, doi: 10.1109/TCOMM.2022.3162249.
[11] T. M. Hoang, L. T. T. Huyen, X. N. Tran, and P. T. Hiep, "Outage probability of aerial base station NOMA MIMO wireless communication with RF energy harvesting," *IEEE Internet Things J.*, vol. 9, no. 22, pp. 22874–22886, Nov. 2022.
[12] J. Ouyang, Y. Che, J. Xu, and K. Wu, "Throughput maximization for laser-powered UAV wireless communication systems," in *Proc. IEEE Int. Conf. Commun. Workshops (ICC Workshops)*, May 2018, pp. 1–6.
[13] M.-A. Lahmeri, M. A. Kishk, and M.-S. Alouini, "Stochastic geometry-based analysis of airborne base stations with laser-powered UAVs," *IEEE Commun. Lett.*, vol. 24, no. 1, pp. 173–177, Jan. 2020.
[14] D.-T. Do, A.-T. Le, Y. Liu, and A. Jamalipour, "User grouping and energy harvesting in UAV-NOMA system with AF/DF relaying," *IEEE Trans. Veh. Technol.*, vol. 70, no. 11, pp. 11855–11868, Nov. 2021.
[15] L. Yang, J. Chen, M. O. Hasna, and H.-C. Yang, "Outage performance of UAV-assisted relaying systems with RF energy harvesting," *IEEE Commun. Lett.*, vol. 22, no. 12, pp. 2471–2474, Dec. 2018.
[16] H. Hu, Y. Huang, G. Cheng, Q. Kang, H. Zhang, and Y. Pan, "Optimization of energy efficiency in UAV-enabled cognitive IoT with short packet communication," *IEEE Sensors J.*, vol. 22, no. 12, pp. 12357–12368, Jun. 2022, doi: 10.1109/JSEN.2021.3130581.
[17] C. M. W. Basnayaka, D. N. K. Jayakody, and Z. Chang, "Age-of-information-based URLLC-enabled UAV wireless communications system," *IEEE Internet Things J.*, vol. 9, no. 12, pp. 10212–10223, Jun. 2022, doi: 10.1109/JIOT.2021.3123431.
[18] L. Yuan, N. Yang, F. Fang, and Z. Ding, "Performance analysis of UAV-assisted short-packet cooperative communications," *IEEE Trans. Veh. Technol.*, vol. 71, no. 4, pp. 4471–4476, Apr. 2022.
[19] H. Ren, C. Pan, K. Wang, Y. Deng, M. Elkashlan, and A. Nallanathan, "Achievable data rate for URLLC-enabled UAV systems with 3-D channel model," *IEEE Wireless Commun. Lett.*, vol. 8, no. 6, pp. 1587–1590, Dec. 2019.
[20] K. Wang, C. Pan, H. Ren, W. Xu, L. Zhang, and A. Nallanathan, "Packet error probability and effective throughput for ultra-reliable and low-latency UAV communications," *IEEE Trans. Commun.*, vol. 69, no. 1, pp. 73–84, Jan. 2021.
[21] A. Ranjha and G. Kaddoum, "URLLC facilitated by mobile UAV relay and RIS: A joint design of passive beamforming, blocklength, and UAV positioning," *IEEE Internet Things J.*, vol. 8, no. 6, pp. 4618–4627, Mar. 2021.
[22] S. Solanki, V. Singh, S. Gautam, J. Querol, and S. Chatzinotas, "Short-packet communication assisted reliable control of UAV for optimum coverage range," in *Proc. IEEE Int. Conf. Commun. Workshops (ICC Workshops)*, May 2023, pp. 1–6.
[23] J. Yao, Q. Zhang, and J. Qin, "Joint decoding in downlink NOMA systems with finite blocklength transmissions for ultrareliable low-latency tasks," *IEEE Internet Things J.*, vol. 9, no. 18, pp. 17705–17713, Sep. 2022, doi: 10.1109/JIOT.2022.3156038.
[24] N. P. Le and K. N. Le, "Uplink NOMA short-packet communications with residual hardware impairments and channel estimation errors," *IEEE Trans. Veh. Technol.*, vol. 71, no. 4, pp. 4057–4072, Apr. 2022, doi: 10.1109/TVT.2022.3148124.
[25] D.-D. Tran, S. K. Sharma, S. Chatzinotas, I. Woungang, and B. Ottersten, "Short-packet communications for MIMO NOMA systems over Nakagami-*m* fading: BLER and minimum blocklength analysis," *IEEE Trans. Veh. Technol.*, vol. 70, no. 4, pp. 3583–3598, Apr. 2021.
[26] T.-H. Vu, T.-V. Nguyen, D. B. D. Costa, and S. Kim, "Intelligent reflecting surface-aided short-packet non-orthogonal multiple access systems," *IEEE Trans. Veh. Technol.*, vol. 71, no. 4, pp. 4500–4505, Apr. 2022, doi: 10.1109/TVT.2022.3146856.
[27] C. Yin, R. Zhang, Y. Li, Y. Ruan, T. Li, T. Tao, and D. Li, "Packet re-management-based C-NOMA for URLLC: From the perspective of power consumption," *IEEE Commun. Lett.*, vol. 26, no. 3, pp. 682–686, Mar. 2022.
[28] Y. Zeng, Q. Wu, and R. Zhang, "Accessing from the sky: A tutorial on UAV communications for 5G and beyond," *Proc. IEEE*, vol. 107, no. 12, pp. 2327–2375, Dec. 2019.
[29] J. Holis and P. Pechac, "Elevation dependent shadowing model for mobile communications via high altitude platforms in built-up areas," *IEEE Trans. Antennas Propag.*, vol. 56, no. 4, pp. 1078–1084, Apr. 2008.
[30] *Study on Enhanced LTE Support for Aerial Vehicles*, document TR-36.777, 3GPP, 2017. [Online]. Available: www.3gpp.org/dynareport/36777.htm
[31] A. A. Khuwaja, Y. Chen, N. Zhao, M.-S. Alouini, and P. Dobbins, "A survey of channel modeling for UAV communications," *IEEE Commun. Surveys Tuts.*, vol. 20, no. 4, pp. 2804–2821, 4th Quart., 2018.
[32] S. Yang, Y. Deng, X. Tang, Y. Ding, and J. Zhou, "Energy efficiency optimization for UAV-assisted backscatter communications," *IEEE Commun. Lett.*, vol. 23, no. 11, pp. 2041–2045, Nov. 2019.
[33] T. Hou, Y. Liu, Z. Song, X. Sun, and Y. Chen, "UAV-to-everything (U2X) networks relying on NOMA: A stochastic geometry model," *IEEE Trans. Veh. Technol.*, vol. 69, no. 7, pp. 7558–7568, Jul. 2020.
[34] S. Zeng, H. Zhang, B. Di, and L. Song, "Trajectory optimization and resource allocation for OFDMA UAV relay networks," *IEEE Trans. Wireless Commun.*, vol. 20, no. 10, pp. 6634–6647, Oct. 2021.
[35] Z. Gong, C. Li, F. Jiang, and J. Zheng, "AUV-aided localization of underwater acoustic devices based on Doppler shift measurements," *IEEE Trans. Wireless Commun.*, vol. 19, no. 4, pp. 2226–2239, Apr. 2020.
[36] X. Mu, Y. Liu, L. Guo, J. Lin, and Z. Ding, "Energy-constrained UAV data collection systems: NOMA and OMA," *IEEE Trans. Veh. Technol.*, vol. 70, no. 7, pp. 6898–6912, Jul. 2021.
[37] M. R. Ramzan, M. Naeem, M. Altaf, and W. Ejaz, "Multicriterion resource management in energy-harvested cooperative UAV-enabled IoT networks," *IEEE Internet Things J.*, vol. 9, no. 4, pp. 2944–2959, Feb. 2022.
[38] H. Xiao, H. Jiang, L.-P. Deng, Y. Luo, and Q.-Y. Zhang, "Outage energy efficiency maximization for UAV-assisted energy harvesting cognitive radio networks," *IEEE Sensors J.*, vol. 22, no. 7, pp. 7094–7105, Apr. 2022.
[39] Y. Polyanskiy, H. V. Poor, and S. Verdu, "Channel coding rate in the finite blocklength regime," *IEEE Trans. Inf. Theory*, vol. 56, no. 5, pp. 2307–2359, May 2010.
[40] Z. Zheng, L. Yuan, and F. Fang, "Performance analysis of fountain coded non-orthogonal multiple access with finite blocklength," *IEEE Wireless Commun. Lett.*, vol. 10, no. 8, pp. 1752–1756, Aug. 2021.
[41] L. Yuan, Z. Zheng, N. Yang, and J. Zhang, "Performance analysis of short-packet non-orthogonal multiple access with Alamouti space-time block coding," *IEEE Trans. Veh. Technol.*, vol. 70, no. 3, pp. 2900–2905, Mar. 2021.
[42] X. Lai, T. Wu, Q. Zhang, and J. Qin, "Average secure BLER analysis of NOMA downlink short-packet communication systems in flat Rayleigh fading channels," *IEEE Trans. Wireless Commun.*, vol. 20, no. 5, pp. 2948–2960, May 2021.
[43] M. K. Simon and M.-S. Alouini, *Digital Communication Over Generalized Fading Channels: A Unified Approach to Performance Analysis*. Hoboken, NJ, USA: Wiley, 2000.
[44] A. Papoulis and S. U. Pillai, *Probability, Random Variables and Stochastic Processes*. New York, NY, USA: McGraw-Hill, 2002.
[45] I. S. Gradshteyn and I. M. Ryzhik, *Table of Integrals, Series, and Products*. Cambridge, MA, USA: Academic, 2014.

TRAN MANH HOANG received the B.S. degree in communication command from Telecommunications University, Ministry of Defense, Nha Trang, Khanh Hoa, Vietnam, in 2002, the B.Eng. degree in electrical engineering from Le Quy Don Technical University, Hanoi, Vietnam, in 2006, the M.Eng. degree in electronics engineering from the Posts and Telecommunications Institute of Technology, Ho Chi Minh City, Vietnam, in 2013, and the Ph.D. degree from Le Quy Don Technical University, in 2018. He is currently a Lecturer with Telecommunications University. He was a Visiting Professor of the School of Information and Communication Engineering, Chungbuk National University, South Korea, from December 2021 to April 2023. He has more than 80 papers in refereed international journals and conferences. His research interests include energy harvesting, UAV, short packet communication, non-orthogonal multiple access, MIMO, RIS, and signal processing for wireless cooperative communications. He was a recipient of the IEEE ATC2022 Best Paper Award.

LE THE DUNG (Member, IEEE) received the B.S. degree in electronics and telecommunication engineering from the Ho Chi Minh City University of Technology, Ho Chi Minh City, Vietnam, in 2008, and the M.S. and Ph.D. degrees in electronics and computer engineering from Hongik University, Seoul, South Korea, in 2012 and 2016, respectively. From 2007 to 2010, he was with Signet Design Solutions, Vietnam, as a Hardware Design Engineer. He was with Chungbuk National University, as a Postdoctoral Research Fellow, from May 2016 to December 2022. Since September 2022, he has been with FPT University, HCMC Campus, as a Lecturer and a Researcher. At the same time, he also has been with RMIT University, Vietnam, as a Teaching Assistant. He has more than 80 papers in refereed international journals and conferences. His major research interests include routing protocols, network coding, network stability analysis and optimization in mobile ad hoc networks, cognitive radio ad hoc networks, and visible light communication networks. He was a recipient of the IEEE IS3C2016 Best Paper Award.

BA CAO NGUYEN received the B.S. degree in electrical engineering from Telecommunication University, Khanh Hoa, Vietnam, in 2006, the M.S. degree in electrical engineering from the Posts and Telecommunications Institute of Technology, Ho Chi Minh City, Vietnam, in 2011, and the Ph.D. degree in electrical engineering from Le Quy Don Technical University, Hanoi, Vietnam, in 2020. He is currently a Lecturer with Telecommunications University. From May 2021 to July 2022, he was with Chungbuk National University, Cheongju, South Korea, as a Postdoctoral Research Fellow. His research interests include energy harvesting, full-duplex, spatial modulation, NOMA, MIMO, RIS, UAV, and cooperative communication.

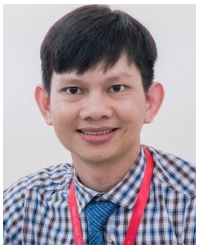

NGUYEN VAN VINH was born in Binh Dinh, Vietnam, in 1984. He received the B.E. degree in computer science from Nha Trang University, Vietnam, in 2008, and the master's degree in computer science from the University of Transport and Communications, Vietnam. He is currently a Lecturer with the Department of Information Assurance (IA), FPT University, Ho Chi Minh City, Vietnam. His research interests are wireless communication in 5G, networking, cybersecurity, physical layer security, and NOMA.

TAEJOON KIM (Member, IEEE) received the B.S. degree in electronics engineering from Yonsei University, Seoul, Republic of Korea, in 2003, and the Ph.D. degree in electrical engineering from the Korea Advanced Institute of Science and Technology (KAIST), Daejeon, Republic of Korea, in 2011. He is currently a Full Professor with the School of Information and Communication Engineering, Chungbuk National University, Cheongju, Republic of Korea. From 2003 to 2005, he was a Researcher with LG Electronics, Seoul. From 2011 to 2013, he was a Senior Researcher with the Electronics and Telecommunications Research Institute (ETRI), Daejeon. His research interests include communication theory and analysis and optimization of wireless networks.